Ultra-slow Li ion dynamics in Li_2C_2—on the similarities of results from ^7Li spin-alignment echo NMR and impedance spectroscopy

2010 J. Phys.: Condens. Matter 22 245901

(http://iopscience.iop.org/0953-8984/22/24/245901)

IOP Publishing Journal of Physics: Condensed Matter

J. Phys.: Condens. Matter **22** (2010) 245901 (10pp) doi:10.1088/0953-8984/22/24/245901

Ultra-slow Li ion dynamics in Li_2C_2—on the similarities of results from ^7Li spin-alignment echo NMR and impedance spectroscopy

B Ruprecht[1], H Billetter[2], U Ruschewitz[2] and M Wilkening[1]

[1] Institute of Physical Chemistry and Electrochemistry, Leibniz University Hannover, Callinstraße 3a, D-30167 Hannover, Germany
[2] Department of Chemistry, Inorganic Chemistry, University of Cologne, Greinstraße 6, D-50939 Köln, Germany

E-mail: uwe.ruschewitz@uni-koeln.de, wilkening@pci.uni-hannover.de and www.wilkening.pci.uni-hannover.de

Received 30 March 2010, in final form 30 April 2010
Published 26 May 2010
Online at stacks.iop.org/JPhysCM/22/245901

Abstract

Li diffusion and transport parameters of binary lithium carbide Li_2C_2 were complementarily investigated by ^7Li (nuclear magnetic resonance) NMR and impedance spectroscopy. Long-range Li diffusion parameters were measured by using mixing-time-dependent and temperature-variable stimulated echo NMR spectroscopy. The method is sensitive to ultra-slow Li hopping processes which were probed from an atomic-scale point of view. Two-time phase correlation functions S_2 obtained can be parameterized by stretched exponentials only. The corresponding echo decay rates τ^{-1}, which were recorded at a resonance frequency of e.g. 155.5 MHz, show Arrhenius behaviour revealing an activation energy of 0.80(2) eV. This value is in very good agreement with that deduced from dc conductivity measurements (0.79(2) eV) probing Li transport processes on a macroscopic length scale. The comparison of impedance data with the measured NMR echo decay functions showed that both methods reflect diffusion processes being characterized by very similar motional correlation functions.

(Some figures in this article are in colour only in the electronic version)

1. Introduction

Diffusion processes are omnipresent phenomena in materials science [1–4] and play a key role in the development of fuel cells [5, 6], batteries [7–13] as well as electrochromic devices [14] and capacitors [15]. In such applications, fast ion conductors are needed. Currently, tremendous efforts are underway to develop materials with improved transport parameters. However, in some research areas materials with very low diffusion coefficients are required. In particular, this is important in some areas of nanoscience. Slow diffusion processes can prevent grain growth and structural relaxation so that metastable nm-sized architectures can be preserved even at high temperatures. Hence, there is also interest in having techniques available which are sensitive to extremely slow diffusion processes. Moreover, for a reliable determination of diffusion parameters in solids it is advantageous to study dynamic processes over a large dynamic range as well as on different times scales [16–21]. Thus, it proves beneficial to extend the accessible dynamic time window down to the regime of ultra-slow motion [16, 22–28].

Amongst the techniques which have been successfully employed to investigate dynamic processes in solids [3, 4], nuclear magnetic resonance (NMR) is ideally suited to study, e.g., jump processes of small cations and anions such as H, Li and F [29, 30]. Whereas NMR spin–lattice relaxation (SLR) techniques are sensitive to very fast dynamic processes characterized by jump rates with values in the MHz and GHz range [30], motions with rates down to 10^4 s^{-1} are detectable by SLR measurements taking advantage of spin-

locking procedures. Between these methods NMR field-cycling relaxometry represents an elegant method to study dynamic phenomena such as rotational and translational motions, see, e.g., [31–33]. The technique has been very successfully applied to characterize dynamic processes such as hydrogen bond dynamics in inorganic and organic liquids, liquid crystals, oligomers and polymers as well as proton glasses, for example [31–33]. Less frequently it has been used to investigate jump processes of ions in metals as well as ionic crystals [33]. In particular, fluorine dynamics in the anion conductor LaF_3 have been studied by spin–lattice relaxation dispersion [34, 35].

Even slower exchange processes with rates smaller than 10^4 s^{-1} can be monitored by two-dimensional (2D) NMR [36–41]. However, in many cases Li 2D exchange NMR experiments are not applicable since a sufficient resolution of NMR lines with distinct chemical shifts cannot be achieved even at extremely large spinning frequencies. In particular, this is the case when diamagnetic instead of paramagnetic Li compounds are to be studied. In the latter, advantage is taken of large site-specific hyperfine shifts extending over a range of some hundreds of ppm. The hyperfine shifts are due to Fermi-contact interactions leading to well resolved NMR signals in many cases. As a result the direct observation of exchange processes by both ^{7}Li and ^{6}Li 2D NMR experiments has become possible [38–41]. Of course, such interactions are absent in the case of diamagnetic compounds where ^{6}Li NMR chemical shifts span a narrow range of only few ppm. Moreover, it is worth noting that in many materials under study the mobile ions regularly occupy just one crystallographic position so that the NMR spectrum consists of a single line only. Irrespective of the spin interaction used to label the ions, this rules out the use of 2D NMR from the outset.

In the present investigation advantage has been taken of the motion-induced decay of ^{7}Li NMR stimulated echoes [16, 18, 23, 24, 29] which are sensitive to ultra-slow Li hopping processes with jump rates lower than 10^4 s^{-1}. Recently, the spin-alignment echo (SAE) NMR technique has also been applied to other Li ion conductors. Interestingly, by the analysis of NMR stimulated echo amplitudes damped by diffusion processes, long-range Li transport parameters can be measured from a microscopic, i.e., atomic-scale point of view [21]. So far, only a few studies [21, 42, 43] can be found in the literature where diffusion parameters obtained from SAE NMR are directly compared with transport parameters probed by dc as well as ac conductivity measurements [44, 45]. The latter are widely used to study the electrical processes occurring in a system on applying an ac signal across the sample pellet. The technique is based on analysing the electrical response of the system, usually after a sinusoidal perturbation. The complex impedance, conductivity or permittivity is generally calculated as a function of the frequency of this perturbation.

Lithium carbide, Li_2C_2, turns out to be another interesting model system for such a comparison since Li motional correlation rates can be detected by SAE NMR measurements. To our knowledge dynamic processes in lithium-rich carbides have hardly ever been studied so far. Previously, ^{13}C NMR was used to characterize the structural details of Li_2C_2 [46].

Li_2C_2 can be directly prepared from the elements [47] and belongs to a large family of lithium carbon materials including lithium-rich (Li_4C, Li_6C_2, Li_8C_3, Li_4C_3, and Li_4C_5) and graphite intercalation compounds (LiC_6, LiC_{12}, LiC_{18}). Below approximately $T' = 770$ K, Li_2C_2 crystallizes with the space group $Immm$ ($Z = 2$). The lattice constants are $a = 365.20(1)$ pm, $b = 483.12(2)$ pm, and $c = 543.44(1)$ pm [47]. Above T' it undergoes a first-order phase transition and becomes cubic (space group $Fm\bar{3}m$). The cubic modification, which can be described as an antifluorite structure, is characterized by disordered C_2^{2-} dumbbells. The crystal structure of the low-temperature modification of Li_2C_2, which is isotypic to Rb_2O_2 and Cs_2O_2, is shown in figure 1. Li ions occupy the 4j sites ($x = 0$, $y = 0.5$, $z = 0.2360(2)$) and C atoms reside on the 4g sites ($x = 0$, $y = 0.1269(2)$, $z = 0$). The shortest Li–Li distance is about 256.5 pm [47].

2. Experimental details

Samples of Li_2C_2 were prepared according to the following protocol, which is slightly different to the one given in the literature [47]. Stoichiometric amounts of lithium and graphite, which was heated in vacuum at 1073 K for 24 h prior to the reaction, were transferred into a purified Ta ampoule. Afterwards the ampoule was sealed in He atmosphere (800 mbar) and was placed inside a quartz ampoule, which was sealed under vacuum. The quartz ampoule was heated for 24 h at 1073 K in air. The sample was allowed to cool down by switching off the furnace. The phase purity of the sample was checked by x-ray powder diffraction (XRPD, Huber G670, Cu Kα_1 radiation, capillary). Apart from a negligible amount of elemental lithium, which was revealed only by ^{7}Li NMR (see section 3), no impurities were detected by XRPD.

^{7}Li NMR stimulated echoes were recorded on Bruker spectrometers (a modified MSL 100 as well as an MSL 400) designed for measurements on solids. The MSL 100 spectrometer, which is equipped with a Kalmus preamplifier, is connected to a field-variable (0–8 T) Oxford cryomagnet. With this setup ^{7}Li NMR measurements were carried out at 77.7 MHz. The MSL 400 spectrometer is used in combination with a shimmed Oxford magnet of fixed field of 9.4 T corresponding to a ^{7}Li resonance frequency of 155.5 MHz. Standard probes were used for the NMR measurements. The 90° pulse length θ_{pulse} of the broadband probe used at 77.7 MHz was 9 μs. θ_{pulse} of the probe connected to the MSL 400 is by a factor of three smaller ($\theta_{\mathrm{pulse}} = 2.8$ μs). In both cases θ_{pulse} slightly depends on temperature. The temperature in the sample chamber is controlled by an Oxford ITC using a stream of heated air or freshly evaporated nitrogen to an accuracy of ±2 K. A Ni–CrNi thermocouple was used to monitor the temperature. The pulse sequence introduced by Jeener and Broekaert, 90°_X–t_{p}–45°_Y–t_{m}–45°–t [48, 49] was used to sample NMR echoes at fixed preparation time $t_{\mathrm{p}} = 10$ μs and variable mixing time t_{m} ranging from 100 μs to 10 s; see [18–20, 29, 49, 50] for both an introduction to the theoretical background of the NMR method as well as technical details. Proper phase cycling was employed to suppress any unwanted coherences [25]. ^{7}Li NMR spin–lattice

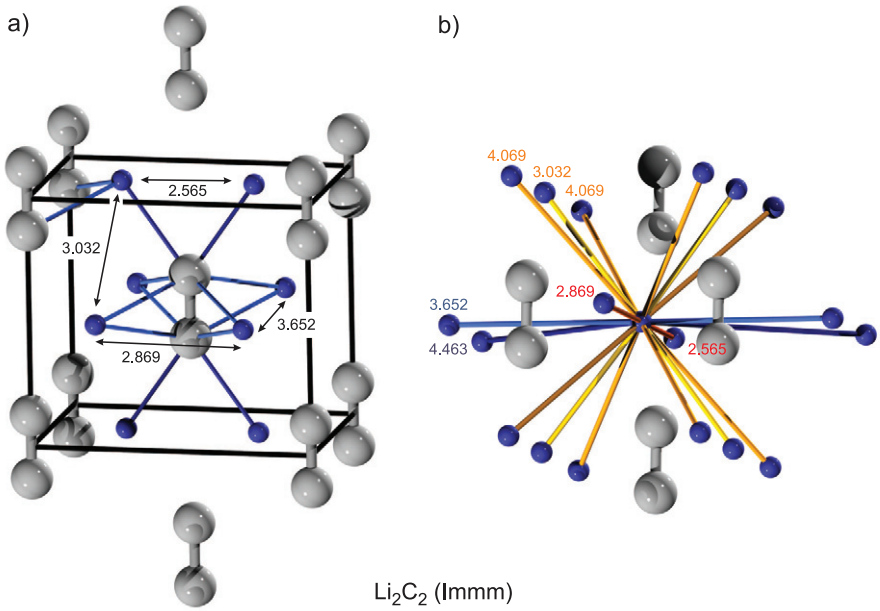

Figure 1. Left: crystal structure of the low-T modification of Li_2C_2 (space group $Immm$). Blue spheres denote Li cations and grey spheres represent the carbon atoms, which form C_2 dumbbells. Selected Li–Li interatomic distances are given in Å. Right: coordination sphere of Li in Li_2C_2. Each Li ion has six Li neighbours with Li–Li distances smaller than or equal to about 3 Å.

relaxation rates T_1^{-1} were acquired with the saturation recovery pulse sequence [51]. The sample was strictly kept under inert-gas atmosphere and handled in a glove box. For the NMR measurements it was carefully fire-sealed in a quartz tube of 3 cm in length and 5 mm in outer diameter.

For the impedance spectroscopy measurements, an HP 4192 A analyzer connected to a home-built cell and working in the frequency range from $f = 5$ Hz to 13 MHz was employed. Conductivity jigs with a four terminal configuration were used. The powdered sample was pressed to cylindrical pellets (8 mm in diameter and 1 mm in thickness) at room temperature. If not stated otherwise, this was done by applying an uniaxial pressure of about 1 GPa. Electrodes were applied by pressing the sample between Pt powder. Impedance measurements were carried out in an inert-gas atmosphere, as well. Calculations of the conductivity, permittivity and electric modulus from the raw data were carried out separately taking into account the dimensions of the sample. The data were carefully analysed with respect to polarization effects (see section 3).

3. Results and discussion

In figure 2 the room temperature ^{7}Li NMR spectrum of Li_2C_2 is shown which was recorded at an external magnetic field of 9.4 T. The dipolar-broadened NMR spectrum, acquired under static, i.e., non-rotating conditions, consists of a central transition flanked by quadrupolar satellite intensities showing the typical powder pattern which is expected for a quadrupole nucleus such as ^{7}Li with a spin-quantum number I of 3/2; see also [18, 52]. In the temperature range (290–473 K) where SAE NMR measurements are carried out to record two-time correlation functions (*vide infra*) no significant changes of the NMR line shape are observed. This clearly indicates that Li jump rates τ^{-1} are much smaller than approximately 10^4 s^{-1}. Here, the rigid lattice line width ζ_{rl} of the central transition $\pm 1/2 \leftrightarrow \mp 1/2$ amounts to being approximately 9.8 kHz. In general, if τ^{-1} reaches the order of ζ_{rl}, dipole–dipole interactions are increasingly averaged due to Li motions on a ms timescale, resulting in a narrowed NMR line; see, e.g., [42, 53] for other examples. In the case of lithium carbide such a motional narrowing is expected to take place at elevated T. Indeed, at 573 K the line width of the central transition is significantly reduced (figure 2(b)) and at 623 K homonuclear dipole–dipole interactions are completely averaged (figure 2(c)). ζ as a function of temperature is shown in figure 3(a). It can be clearly seen that motional narrowing starts at temperatures somewhat higher than 473 K. Thus, below this so-called onset temperature ultra-slow Li motions take place in Li_2C_2.

From the satellite singularities adjacent to the central line of the ^{7}Li NMR spectra (figure 2) the quadrupole coupling constant C_{q} characterizing the interaction of the quadrupole moment of ^{7}Li with a non-vanishing electric field gradient (EFG) at the site (4j) of the Li spins in Li_2C_2 can be determined. If an axially oriented electric field gradient (with respect to the principal axis system defined by the direction of the external magnetic field) is assumed, no simulation is needed to extract the constant C_{q}. In such a case it is simply twice the distance $\Delta\nu$ between the quadrupole singularities, as indicated in figure 2. Here, C_{q} amounts to be 51.9(2) kHz at room temperature. Certainly, this value does not take into account (local) field gradients which are governed by, e.g., point defects in Li_2C_2. As can be seen in figure 2, a very small amount of metallic Li is present in the sample, which shows up at $\delta = 261(1)$ ppm, being the typical Knight-shift of lithium [54, 55].

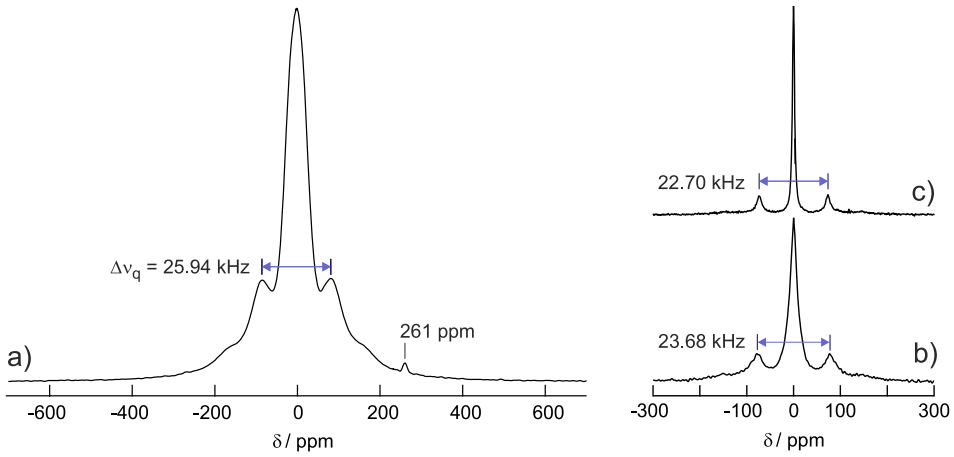

Figure 2. (a) ^{7}Li NMR spectrum of Li_2C_2 recorded at 291 K. The resonance frequency was 155.5 MHz, which corresponds to an external magnetic field of 9.4 T. The spectrum is referenced to aqueous LiCl. The very weak NMR signal at $\delta = 261$ ppm is due to residual metallic Li. (b) and (c) ^{7}Li NMR spectra of Li_2C_2 recorded at 573 and 623 K, respectively. Starting from room temperature (rigid lattice regime) the quadrupole coupling constant $C_q = 2\Delta\nu_q$ decreases by approximately 12% when T is increased to 623 K (regime of extreme narrowing).

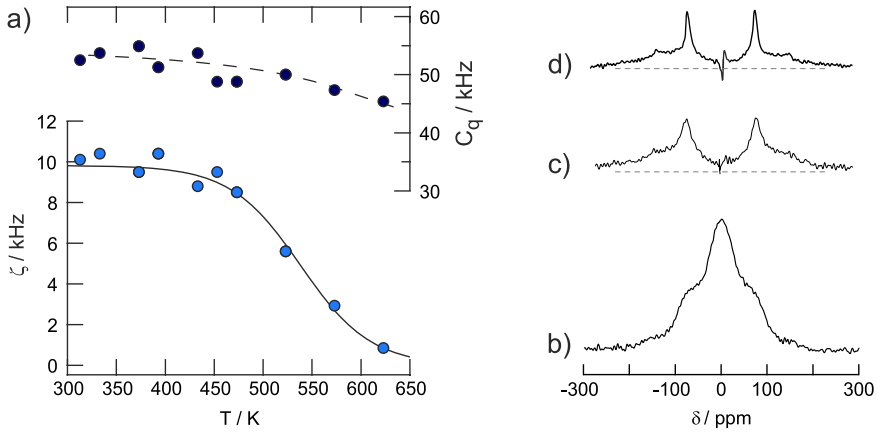

Figure 3. (a) Temperature dependence of the ^{7}Li NMR line width ζ as well as that of the quadrupole coupling constant C_q; (b)–(d): ^{7}Li spin-alignment echo NMR spectra ($t_p = 10$ μs and $t_m = 100$ μs) of Li_2C_2 which were recorded at various temperatures namely (b) 300 K, (c) 573 K and (d) 623 K. The spectra were recorded at 155.5 MHz. They were obtained by Fourier transformation of the corresponding echoes starting at the top showing up at $t = t_p$.

Interestingly, C_q slightly depends on temperature (figure 3(a)). Fitting artefacts of the NMR spectra can be ruled out in explaining this observation. Increasing T to 623 K leads to a decrease of C_q from 51.9(2) to 45.4(1) kHz. This might be attributed to a small increase of the lattice parameters of Li_2C_2 [47, 56]. The shape of the ^{7}Li NMR spectrum recorded at $T = 623$ K gives strong evidence that the EFG is axially symmetric; see, e.g., also [57].

In order to probe extremely slow Li dynamics, which are, below 473 K, detectable neither by NMR line shape nor spin–spin relaxation measurements, stimulated echo NMR experiments are carried out. Such measurements are sensitive to Li hopping processes with jump rates smaller than 10^4 s^{-1}. ^{7}Li SAE NMR spectra are shown in figure 3 for various temperatures. In contrast to the spectra displayed in figure 2, the satellite intensities arising from quadrupole interactions are greatly increased. An ideal spin-alignment spectrum, for which homonuclear dipole–dipole interactions are absent, consists of these components only. However, in many cases central intensities show up at lower temperatures, reflecting ^{7}Li–^{7}Li dipolar couplings. This feature was rationalized by modelling of SAE NMR spectra, taking into account sufficiently strong dipolar interactions [25]. The more effective these couplings are averaged with increasing T, the more the SAE NMR spectrum is governed by the $\pm 3/2 \leftrightarrow \pm 1/2$ transitions (see figure 3(d)), see also [24].

In figure 4(a) ^{7}Li NMR stimulated echo decay curves $S_2(t_p, t_m, t = t_p)$ are shown which were recorded at the temperatures indicated. $S_2(t_p, t_m, t = t_p)$ represents the decrease of the echo amplitude with increasing mixing time t_m. Amplitudes were always read out at $t = t_p$, i.e., where the top of the NMR echo appears. The curves, normalized to range between 0 and 1, can only be represented by stretched exponentials

$$S_2 = \exp(-(t_m/\tau_{echo})^{\gamma}). \quad (1)$$

Above $T = 433$ K the exponent γ has reached a constant value of approximately 0.55. Below this temperature the

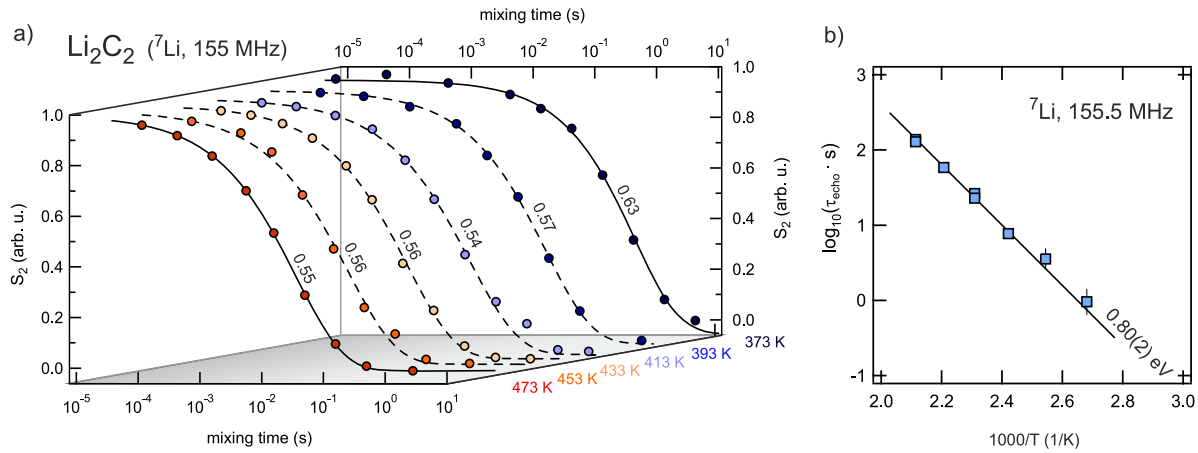

Figure 4. Left: temperature-dependent ^{7}Li NMR decay curves $S_2(t_p, t_m, t = t_p)$ which were obtained by reading out the amplitude at $t = t_p$ of a series of stimulated echoes recorded at different mixing times t_m. Data were recorded at a resonance frequency of 155.5 MHz. Solid and dashed lines are fits with stretched exponential functions. The stretching exponents γ are indicated. Right: Arrhenius plot of the ^{7}Li NMR decay rates τ_{echo}^{-1}. From the slope of the fit (solid line), an activation energy of approximately 0.8 eV can be deduced.

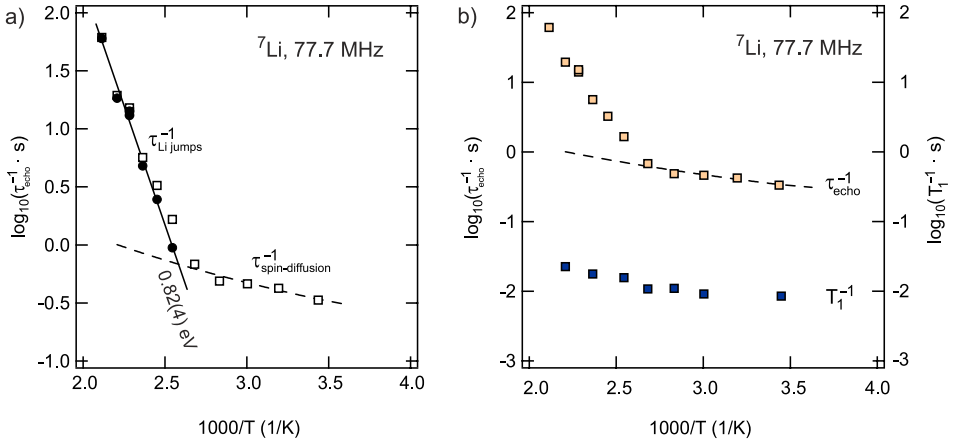

Figure 5. Decay rates τ_{echo}^{-1} of Li_2C_2 which were recorded at 77.7 MHz down to $T = 291$ K. Below $T \approx 350$ K background rates show up following a power law $T_1^{-1} \propto T^{\kappa}$ with $\kappa = 1.9$ (dashed line). Decay rates purely controlled by Li diffusion are obtained by subtracting the background rates from the overall τ_{echo}^{-1} values measured at higher T. See text for further details.

stretching of the echo decay curves is characterized by a γ value somewhat larger than 0.6. In figure 4(b) the corresponding rates τ_{echo}^{-1} are shown in an Arrhenius representation. According to

$$\tau_{echo}^{-1} \propto \exp(-E_a/(k_B T)), \tag{2}$$

where E_a denotes the activation energy and k_B Boltzmann's constant, $E_a = 0.80(2)$ eV is obtained. The same value is found (0.80(3) eV) when temperature-variable ^{7}Li NMR stimulated echoes recorded at 77.7 MHz are analysed which were additionally corrected for any interfering weaker-than-activated background effects showing up at $T < 350$ K. The corresponding decay rates are plotted versus inverse temperature in figure 5. As can be clearly seen, below approximately 350 K echo damping is controlled by a weaker-than-activated process with a mean decay rate τ_{echo}^{-1} of about 2 s^{-1}. This indicates that $S_2(t_p, t_m, t = t_p)$ is most likely influenced by, e.g., spin-diffusion effects rather than by mass transport in this low-T regime. Especially in materials with short Li–Li distances (see figure 1), spin-diffusion effects are expected to play an important role at low temperatures. In order to quantify the influence of the detected background rates on echo damping at higher T, we fitted the rates in the low-T regime with a power law according to

$$\tau_{echo}^{-1} \propto T^{\kappa}. \tag{3}$$

Here, the power-law exponent κ turns out to be about 1.9. Let us mention that a quadratic temperature dependence is also expected for NMR spin–lattice relaxation processes induced by lattice vibrations. Thus, one might assume that the background rates detected reflect the superposition of non-diffusive influences on echo decay. Subtracting the extrapolated rates from those measured at high temperatures, see also [58], yields background-corrected SAE NMR decay rates (filled symbols in figure 5(a)) which follow an Arrhenius law with an activation energy of 0.80(3) eV.

In the absence of any interfering influences such as spin-diffusion effects, the lower limit of detectable τ_{echo}^{-1} rates is

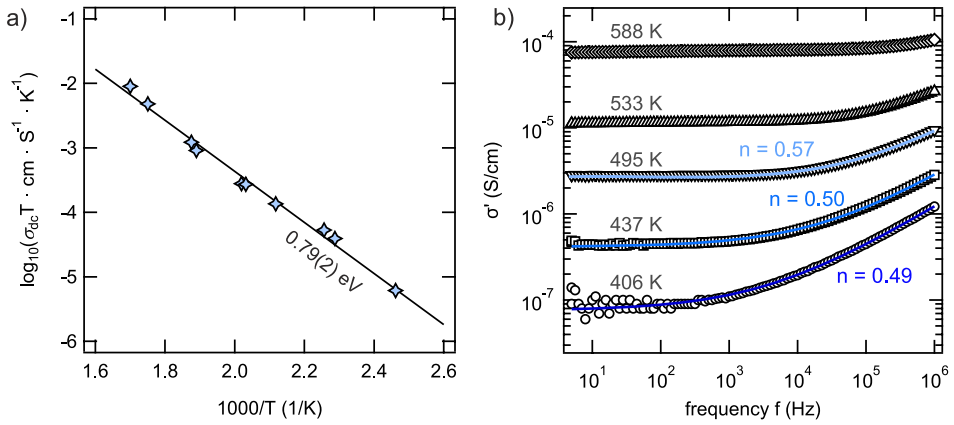

Figure 6. (a) Temperature dependence of σ_{dc} of the low-T modification of Li_2C_2. The solid line represents a fit according to an Arrhenius relation. (b) Temperature-variable impedance spectra of Li_2C_2 which are composed of distinct dc-plateaus and a dispersive regime showing up at low temperature and high frequencies. Solid lines show fits using a power law $\sigma' = \sigma_{dc} + A_0\omega^n$.

generally expected to be given by the quadrupolar SLR rate T_{1Q}^{-1} (see [29, 58] for general outlines of T_{1Q}), which is, provided the dominant relaxation mechanism is of quadrupolar nature, predicted to be about 25/8 of that of the longitudinal (Zeeman) NMR relaxation rate T_1^{-1} [58]. Indeed, as shown by Böhmer *et al*, a ratio of approximately three has been found for T_1^{-1}/T_{1Q}^{-1} in some cases [58]. However, there are also examples known where this ratio is four times larger than the expected value [58]. In the present study, T_1^{-1} is by about a factor of 40 larger than τ_{echo}^{-1} measured at 291 K, for example. This clearly limits the Li stimulated echo NMR technique to detect decay rates smaller than $\tau_{echo}^{-1} = 1\ s^{-1}$. On the other hand, interfering non-diffusion controlled effects can be well separated from the data of interest here.

It is worth noting that the ^{7}Li NMR magnetization transients $M(t)$ cannot be represented by a single exponential. Instead, $M(t)$ is well approximated with the help of a stretched exponential,

$$M(t) \propto \exp(-(t/T_1)^{\gamma_{SLR}}) \tag{4}$$

with γ_{SLR} only slightly depending on temperature in the T range covered here. $\gamma_{SLR} \approx 0.69$ is found at low T; the value steadily increases to about 0.75 at $T = 473$ K. Thus, γ_{SLR} determined at low temperatures is similar to the stretching exponent found for the stimulated echo decay at $T = 393$ K. Deviations of $M(t)$ from purely exponential time behaviour are expected for a spin-3/2 nucleus, such as ^{7}Li, if, for example, a quadrupolar relaxation mechanism is mainly responsible for the recovery of $M(t)$ [59].

Interestingly, the activation energy E_a probed is very similar to that which can be deduced from electrical impedance measurements. In figure 6 the temperature dependence of the ionic dc conductivity σ_{dc} is shown according to the Arrhenius relation

$$\sigma_{dc}T = \sigma_0 \exp(-E_{a,dc}/(k_B T)). \tag{5}$$

The solid line in figure 6 corresponds to an activation energy of $E_{a,dc} = 0.79(2)$ eV, reflecting long-range ionic motion in Li_2C_2. The good agreement of the two values deduced from NMR on the one hand and dc conductivity measurements on the other hand strongly suggests that Li ions are the dominant charge carriers. In contrast to the impedance spectroscopy measurements performed here, stimulated echo NMR is selectively sensitive to Li jumps.

σ_{dc} values were determined from the frequency independent plateaus of the corresponding impedance spectra $\sigma'(f)$, which are shown for various temperatures in figure 6(b). At low temperatures and high frequencies the dispersive regime of $\sigma'(f)$ shows up. Any remarkable polarization effects due to the Pt electrodes applied, which block Li transport, are absent. However, such effects are clearly seen when the permittivity ε' is plotted as a function of frequency (*vide infra*). At 500 K the conductivity of Li_2C_2 measured is 6.3×10^{-7} S cm^{-1}, which is a typical value of a poor ionic conductor.

The shape of the impedance spectra of figure 6 can be roughly described by a power law

$$\sigma' = \sigma_{dc} + A_\sigma \omega^n \tag{6}$$

at least in the frequency range covered here. The exponent n usually ranges between 0 and 1. From 400 to 500 K the power-law exponent n is found to be in the range $0.49 \leqslant n \leqslant 0.57$. For comparison, in the case of structurally disordered materials, values around $n = 2/3$ are often found. It is worth noting that the better the dispersive ac regime can be detected, i.e., the lower T is chosen, the more precise the exponent n can be determined from suitable fits. n can be linked to the kind of underlying correlation function describing the electrical response. In the most practicable way a stretched exponential

$$\phi(t) = \exp(-(t/\tau')^\beta) \tag{7}$$

is assumed to take into account the deviations from the ideal Debye response being characterized by a pure exponential correlation function ($\beta = 1$). In general, it can be shown that $\phi(t)$ represents a good approximation of the velocity correlation function $G_\sigma(t)$ of ion conductors showing correlated motions of the charge carriers [60]. The Fourier transform of $G_\sigma(t)$ gives the complex conductivity. Stretched correlation functions are expected for structurally disordered ion conductors where β can be related to the distribution width of electrical relaxation frequencies characterizing the

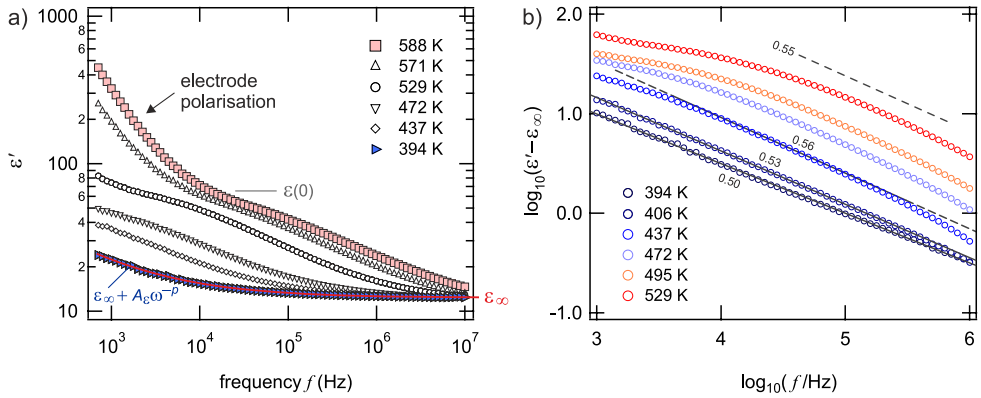

Figure 7. (a) Real part ε' of the complex permittivity $\hat{\varepsilon}$ of Li_2C_2 as a function of frequency. The curves were recorded at the temperatures indicated. (b) The ac part of the permittivity plotted as $\varepsilon' - \varepsilon_\infty$ versus frequency. Partly, the slopes of the linear fits performed are indicated. For example, $p \approx 0.55$ is obtained in the temperature regime.

impedance response measured, see, e.g., [61]. Interestingly, in the present case, an exponent $\beta_n = 1 - n = 0.50$ is obtained at 437 K, which is in good agreement with $\gamma = 0.56$ ($T = 433$ K) obtained by measuring the motional correlation functions directly using SAE NMR spectroscopy. γ values of about 0.55 are found in the temperature range where slow Li motions dominate the S_2 echo decay. It should be noted that γ remains the same even when correlation functions $S_{2,\mathrm{corr.}} = S_2/S_{2,293\ \mathrm{K}}$ corrected for background effects are examined. $S_{2,\mathrm{corr.}}$ takes into account the contribution of the non-diffusion-induced low-T decay curve $S_{2,293\ \mathrm{K}}$. We refer to [50], where this correction procedure is described in detail. It becomes more important when the two regions smoothly merge into each other, which is, however, not the case here. As can be seen from figures 4 and 5, above 433 K the SAE NMR data, i.e., τ^{-1} as well as γ, are hardly influenced by background effects.

As mentioned above, γ values smaller than one might be explained in terms of a distribution of jump rates. Alternatively, the hopping correlation function can intrinsically be of non-exponential nature. For example, the latter might be found for ion conductors providing migration pathways of low dimensionality, i.e., where diffusion is highly anisotropic [16]. A molecular dynamics simulation in combination with results from three- and four-time NMR correlation functions, see, e.g,. [62–65], might be helpful in accepting the challenge to interpret the stretching exponent from an atomistic point of view.

Besides the complex conductivity $\hat{\sigma}$, the permittivity $\hat{\varepsilon}$ can also be used to shed light on the shape of the underlying electrical correlation function. In figure 7(a) the real part of $\hat{\varepsilon}$ is plotted as a function of frequency. Electrode polarization effects which are due to the formation of space–charge layers show up at low frequencies and high temperatures. They are marked by an arrow. At sufficiently large frequencies and low temperatures ($T = 394$ K) blocking effects due to electrode polarization are largely reduced and $\varepsilon'(\omega)$ can be roughly described by the power law [66]

$$\varepsilon'(\omega) = \varepsilon_\infty + A_\varepsilon \omega^{-p} \tag{8}$$

with $\lim_{\omega\to\infty} \varepsilon' \equiv \varepsilon_\infty = 12.3(3)$ being the high frequency permittivity and an exponent $p \approx 0.5$ comparable with γ. Certainly, due to the onset of interfering electrode polarization effects, the determination of p at higher T is fraught with difficulties. This can be seen when the difference $\varepsilon' - \varepsilon_\infty$ is plotted versus frequency (figure 7(b)). p is related to n via $p = 1 - n$ [66]. It slightly increases with increasing T, revealing a good agreement with the stretching exponent deduced from stimulated echo NMR. The most reliable p values can be obtained at the lowest temperatures of figure 7(b). Finally, the ac storage-to-loss ratio can be used to estimate n. Combination of equations (6) and (8) yields

$$\frac{\omega(\varepsilon' - \varepsilon_\infty)}{\sigma' - \sigma_{\mathrm{dc}}} = \frac{A_\varepsilon}{A_\sigma}\omega^{1-n-p} = \tan(n\pi/2) \tag{9}$$

where $A_\varepsilon = A_0 \sin(n\pi/2)$ and $A_\varepsilon = A_0 \cos(n\pi/2)$ [66]. $\omega\varepsilon_\infty(\varepsilon' - \varepsilon_\infty)/(\sigma' - \sigma_{\mathrm{dc}})$ versus frequency is shown in figure 8. An ac storage-to-loss ratio of about one is consistent with $n \approx 0.5$, as deduced from analysing the real parts of $\hat{\varepsilon}(\omega)$ and $\hat{\sigma}(\omega)$, respectively.

Moynihan *et al* [67] introduced the stretched exponential correlation function to characterize the width of the modulus peaks [68]

$$M''(\omega) = (\sigma'\omega)/(\varepsilon'^2 + (\sigma'\omega)^2) \tag{10}$$

in an empirical manner. They proposed for $\hat{M} \equiv 1/\hat{\varepsilon} = M' + \mathrm{i}M''$ the expression

$$\hat{M} = 1/\varepsilon_\infty\{1 - L(-\mathrm{d}\phi/\mathrm{d}t)\} \tag{11}$$

where $L(x)$ is the Laplace transform of x. According to that formalism for, e.g., $\beta = 0.56$ a peak width of $\Delta M = 1.95$ decades is expected when M'' is plotted versus $\log(f/\mathrm{Hz})$ [67]. Indeed, the normalized modulus curves M'' of figure 9(b) (the corresponding M' data is shown in figure 9(a)) are characterized by a peak width ΔM (full width at half maximum) of exactly 1.95(1) decades.

Thus, comparing the stretching exponent γ of stimulated echo NMR with results deduced from impedance spectroscopy, a consistent picture of the underlying correlation function is

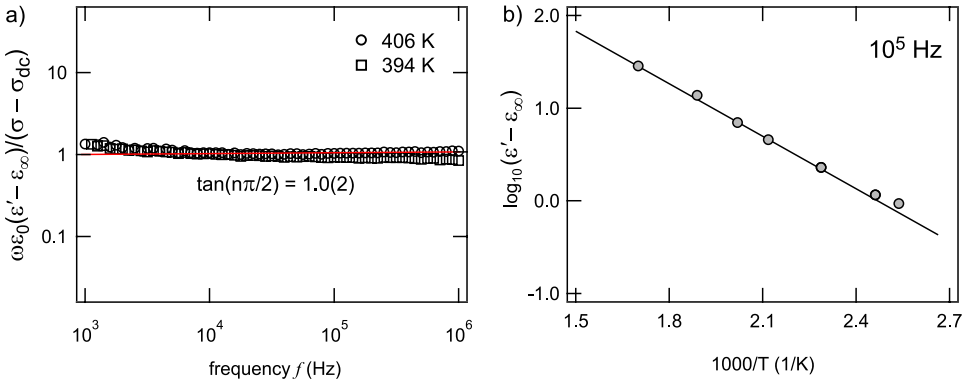

Figure 8. (a) ac storage-to-loss ratio $\omega\varepsilon_\infty(\varepsilon' - \varepsilon_\infty) \cdot (\sigma' - \sigma_{dc})^{-1}$ plotted as a function of frequency. $\tan(n\pi/2) \approx \tan(\pi/4) = 1$ reveals $n \approx 0.5$ at $T \approx 400$ K. (b) Arrhenius plot of $\varepsilon' - \varepsilon_\infty$ determined at $\omega/2\pi = 10^5$ Hz. The solid line is a least-squares fit and yields an ac activation energy of approximately 0.4 eV.

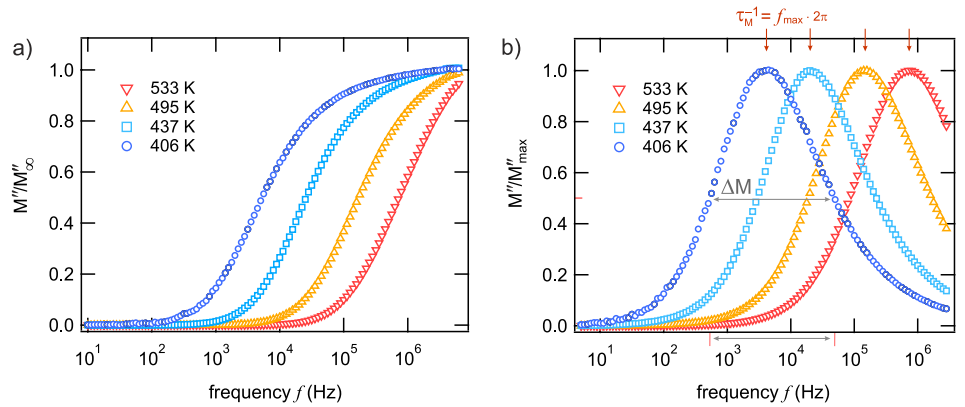

Figure 9. Plot of (a) the real and (b) the imaginary part of the electrical modulus of Li_2C_2 as a function of frequency. A peak width of approximately two decades on the frequency scale corresponds to a KWW stretching exponent (equation (7)) of about 0.55. This is in perfect agreement with the correlation function directly measured by stimulated echo NMR spectroscopy (figure 4).

obtained even when probed on different time scales. This comparison shows that, in the case of Li_2C_2, the primary time-dependent observables of both methods are obviously controlled by the same hopping correlation function. In the case of stimulated echo NMR this is a single-spin correlation function, which is in contrast to, for example, spin–lattice relaxation NMR being governed by a correlation function controlled by magnetic dipole interactions of ion pairs instead [69, 70].

For the sake of completeness, the modulus representation [68] can also be used to extract characteristic relaxation frequencies τ_M^{-1} from the peak positions of the M''-curves. The rates $\tau_M^{-1} = f_{max}2\pi$, where f_{max} is the frequency at which M'' passes through its maximum, coincide with the mean conductivity relaxation rates, which can be calculated from σ_{dc} via $\langle\tau_\sigma^{-1}\rangle = \sigma_{dc}/(\varepsilon_0\varepsilon_\infty)$, where ε_0 is the permittivity of free space. $\langle\tau_\sigma\rangle$ is related to τ' of equation (7) according to $\langle\tau_\sigma\rangle = \beta^{-1}\Gamma(\beta^{-1})\tau'$, where Γ denotes the gamma function. Provided β is independent of temperature, here the corresponding activation energy equals $E_{a,dc}$. Let us note that the use of M'' to analyse impedance data is often criticized [44, 68] because M'' represents an irreversible combination of both the real part of the conductivity and the permittivity which, in contrast to M'', can be measured directly.

Analysing the temperature dependence of ε' and σ' at frequencies 10^5 Hz $\leqslant \omega/2\pi \leqslant 10^6$ Hz, activation energies $E_{a,ac}$ ranging from 0.36(2) to 0.42(3) eV are obtained when $\log(\varepsilon'(\omega) - \varepsilon_\infty)$ is plotted versus the inverse temperature. Thus, the ratio $E_{a,dc}/E_{a,ac} = 2.0(3)$ compares favourably with $1/\beta_n$ as well as $1/\gamma$ obtained by NMR [71, 72]. Let us mention that an activation energy comparable to that of $E_{a,ac}$ is expected to be deduced also from the low-T flank of the diffusion-induced NMR spin–lattice relaxation rate peak of Li_2C_2; see also [42] for comparison. Although we have extended the T_1^{-1} NMR measurements shown in figure 4 up to $T = 623$ K, the low-T flank could not be detected. At 623 K the SLR NMR rate is approximately 3×10^{-2} s^{-1}. Thus, it is still determined by non-diffusion-induced background effects. Note that Li_2C_2 transforms into the cubic modification at approximately 770 K, limiting the application of SLR NMR in order to probe very fast Li jump processes on the μs to ns timescale in the low-temperature modification of lithium carbide.

4. Summary and conclusion

Extremely slow Li self-diffusion in polycrystalline Li_2C_2 was investigated by ^{7}Li stimulated echo NMR. Two-time correlation functions were recorded in the temperature regime

of the rigid lattice. In this T range Li jump rates are expected to take values smaller than 10^3 s^{-1}, so they cannot be determined by conventional NMR line shape measurements, for example. The activation energy probed by NMR is characteristic for long-range Li diffusion, and agrees well with that deduced from macroscopic dc conductivity measurements. Thus, Li_2C_2 serves as an interesting model system to show that SAE NMR is capable to provide access to long-range diffusion parameters probed by the help of a microscopic method.

Interestingly, the comparison with temperature- and frequency-dependent electrical quantities, such as the complex conductivity as well as permittivity, shows that both methods probe Li dynamics which are controlled by the same correlation function, which can be directly measured in the case of stimulated echo NMR. In the future, combined diffusion studies taking advantage of both stimulated echo NMR and impedance spectroscopy might become very helpful to understand the complex electrical responses of ion conductors in general, and Li ion dynamics in structurally disordered materials in particular. Examples are expected to be found for which stimulated echo NMR and conductivity measurements yield different results. For instance, this might include nano-sized systems whose diffusion properties might be influenced by interface effects. Such materials are highly considered to act as promising energy materials in Li ion batteries. Further studies on suitable model substances, which reveal the similarities of both methods without being additionally controlled by a structurally complex microstructure, will build a necessary basis for the identification and reliable interpretation of such effects.

Acknowledgments

We gratefully acknowledge P Heitjans for many fruitful discussions and for allowing us to use his NMR and impedance spectroscopy equipment in Hannover. We thank the Deutsche Forschungsgemeinschaft (research unit 1277 molife (Mobilität von Li-Ionen in Festkörpern) (grant no. WI 3600 2-1 as well as 4-1)) and the Leibniz University Hannover (grant for the project DYNAMA) for financial support.

References

[1] Philibert J 2006 *Diffus. Fundam.* **4** 6.1
[2] Mehrer H and Stolwijk N A 2009 *Diffus. Fundam.* **11** 1
[3] Heitjans P and Kärger J (ed) 2005 *Diffusion in Condensed Matter—Methods, Materials, Models* 2nd edn (Berlin: Springer)
[4] Mehrer H 2006 *Diffusion in Solids* (Berlin: Springer)
[5] Kreuer K D 2001 *J. Membr. Sci.* **185** 29
[6] Kreuer K D 2003 Proton-conducting oxides *Annu. Rev. Mater. Res.* **33** 333–59
[7] Tarascon J M and Armand M 2001 *Nature* **1414** 359
[8] Whittingham M S 2004 *Chem. Rev.* **104** 4271
[9] Novak P, Müller K, Santhanam K S V and Haas O 1997 Electrochemically active polymers for rechargeable batteries *Chem. Rev.* **97** 207
[10] Bruce P G, Scrosati B and Tarascon J-M 2008 *Angew. Chem. Int. Edn* **47** 2930
[11] Aricó A S, Bruce P G, Scrosati B, Tarascon J-M and Van Schalkwijk W 2005 *Nature* **4** 366
[12] Wakihara M and Yamamoto O (ed) 1998 *Lithium Ion Batteries* (Weinheim: Wiley–VCH)
[13] Goodenough J B and Kim Y 2010 *Chem. Mater.* **22** 587
[14] Niklasson G A and Granqvist C G 2007 *J. Mater. Chem.* **17** 127
[15] Brezesinski T, Wang J, Tolbert S H and Dunn B 2010 *Nat. Mater.* **9** 146
[16] Wilkening M and Heitjans P 2008 *Phys. Rev.* B **77** 024311
[17] Wilkening M, Kuhn A and Heitjans P 2008 *Phys. Rev.* B **78** 054303
[18] Wilkening M and Heitjans P 2006 *J. Phys.: Condens. Matter* **18** 9849
[19] Wilkening M, Gebauer D and Heitjans P 2008 *J. Phys.: Condens. Matter* **20** 022201
[20] Wilkening M, Amade R, Iwaniak W and Heitjans P 2006 *Phys. Chem. Chem. Phys.* **9** 1239
[21] Wilkening M, Mühle C, Jansen M and Heitjans P 2007 *J. Phys. Chem.* B **111** 8691
[22] Wilkening M, Küchler W and Heitjans P 2006 *Phys. Rev. Lett.* **97** 065901
[23] Böhmer R, Jörg T, Qi F and Titze A 2000 *Chem. Phys. Lett.* **316** 419
[24] Qi F, Jörg T and Böhmer R 2002 *Solid State Nucl. Magn. Reson.* **22** 484
[25] Qi F, Diezemann G, Böhm H, Lambert J and Böhmer R 2004 *J. Magn. Reson.* **169** 225
[26] Qi F, Rier C, Böhmer R, Franke W and Heitjans P 2005 *Phys. Rev.* B **72** 104301
[27] Tang X-P, Busch R, Johnson W L and Wu Y 1998 *Phys. Rev. Lett.* **81** 5358
[28] Tang X-P, Geyer U, Busch R, Johnson W L and Wu Y 1999 *Nature* **402** 160
[29] Böhmer R, Jeffrey K and Vogel M 2007 *Prog. Nucl. Magn. Reson. Spectrosc.* **50** 87
[30] Heitjans P, Schirmer A and Indris S 2005 *Diffusion in Condensed Matter—Methods, Materials, Models* 2nd edn, ed P Heitjans and J Körger (Berlin: Springer) chapter 9, pp 369–415
[31] Horsewill A J 2008 *Prog. Nucl. Magn. Reson. Spectrosc.* **52** 170
[32] Kimmich R and Anoardo E 2004 *Prog. Nucl. Magn. Reson. Spectrosc.* **44** 257
[33] Noack F 1986 *Prog. Nucl. Magn. Reson. Spectrosc.* **18** 171
[34] Fujara F, Kruk D, Lips O, Privalov A F, Sinitsyn V and Stork H 2008 *Solid State Ion.* **179** 2350 and references therein
[35] Privalov A F, Lips O and Fujara F 2002 *J. Phys.: Condens. Matter* **14** 4515
[36] Xu Z and Stebbins J F 1995 *Science* **270** 1332
[37] van Wüllen L, Echelmeyer T, Meyer H-W and Wilmer D 2007 *Phys. Chem. Chem. Phys.* **9** 3298
[38] Verhoeven V W J, de Scheper I M, Nachtegaal G, Kentgens A P M, Kelder E M and Mulder F M 2001 *Phys. Rev. Lett.* **86** 4314
[39] Cahill L S, Chapman R P, Britten J F and Goward G R 2006 *J. Phys. Chem.* B **110** 7171
[40] Cabana J, Dupré N, Rousse G, Grey C P and Palacin M R 2005 *Solid State Ion.* **176** 2205
[41] Davis L J M, Heinmaa I and Goward G R 2010 *Chem. Mater.* **22** 769
[42] Wilkening M, Epp V, Feldhoff A and Heitjans P 2008 *J. Phys. Chem.* C **112** 9291
[43] Faske S, Eckert H and Vogel M 2008 *Phys. Rev.* B **77** 104301
[44] Sidebottom D L 2009 *Rev. Mod. Phys.* **81** 999
[45] Barsoukov E and MacDonald J R (ed) 2005 *Impedance Spectroscopy—Theory, Experiment and Applications* (Hoboken, NJ: Wiley)
[46] Duncan T M 1989 *Inorg. Chem.* **28** 2663

[47] Ruschewitz U and Pöttgen R 1999 *Z. Allg. Anorg. Chem.* **625** 1599
[48] Jeener J and Broekaert P 1967 *Phys. Rev.* **157** 232
[49] Böhmer R 2000 *J. Magn. Reson.* **147** 78
[50] Wilkening M, Heine J, Lyness C, Armstrong A R and Bruce P G 2009 *Phys. Rev.* B **80** 064302
[51] Fleischer G and Fujara F 1994 *NMR—Basic Principles and Progress* vol 30, ed P Diehl, E Fluck, H Günther, R Kosfeld and J Seelig (Berlin: Springer)
[52] Abragam A 1961 *The Principles of Nuclear Magnetism* (Oxford: Clarendon)
[53] Wilkening M, Iwaniak W, Heine J, Epp V, Kleinert A, Behrens M, Nuspl G, Bensch W and Heitjans P 2007 *Phys. Chem. Chem. Phys.* **9** 6199
[54] Itami T, Shimoji M, Meijer J A and van der Lugt W 1988 *J. Phys. F: Met. Phys.* **18** 2409
[55] Kittel C 1996 *Introduction to Solid State Physics* (New York: Wiley)
[56] Juza R, Wehle V and Schuster H-U 1967 *Z. Allg. Anorg. Chem.* **352** 252
[57] Bredow T, Heitjans P and Wilkening M 2004 *Phys. Rev.* B **70** 115111
[58] Böhmer R and Qi F 2007 *Solid State Nucl. Magn. Reson.* **31** 28
[59] Hubbard P S 1970 *J. Chem. Phys.* **53** 985
[60] Meyer M, Maass P and Bunde A 1993 *Phys. Rev. Lett.* **71** 573
[61] Ngai K L 1996 *J. Non-Cryst. Solids* **203** 232
[62] Vogel M, Brinkmann C, Eckert H and Heuer A 2002 *Phys. Chem. Chem. Phys.* **4** 3237
[63] Vogel M, Brinkmann C, Eckert H and Heuer A 2002 *J. Non-Cryst. Solids* **307** 971
[64] Vogel M, Brinkmann C, Eckert H and Heuer A 2002 *Solid State Nucl. Magn. Reson.* **22** 344
[65] Vogel M, Brinkmann C, Eckert H and Heuer A 2006 *J. Non-Cryst. Solids* **352** 5156
[66] Sidebottom D L, Green P F and Brow R K 1995 *J. Non-Cryst. Solids* **183** 151
[67] Moynihan C T, Boesch L P and Laberge N L 1973 *Phys. Chem. Glasses* **14** 122
[68] Hodge I M, Ngai K L and Moynihan C T 2005 *J. Non-Cryst. Solids* **351** 104
[69] Kanert O, Küchler R, Ngai K L and Jain H 1994 *Phys. Rev.* B **49** 76
[70] Bunde A, Dieterich W, Maass P and Meyer M 2005 *Diffusion in Condensed Matter—Methods, Materials, Models* 2nd edn, ed P Heitjans and J Kärger (Berlin: Springer) chapter 20, pp 813–56
[71] Ngai K L and Martin S W 1989 *Phys. Rev.* B **40** 10550
[72] Ngai K L, Greaves G N and Moynihan C T 1998 *Phys. Rev. Lett.* **80** 1018